Electrical tuning of moiré excitons in MoSe<inf>2</inf> bilayers

Electrical tuning of moiré excitons in $MoSe_2$ bilayers

IOP Publishing 2D Mater. 10 (2023) 014013 https://doi.org/10.1088/2053-1583/aca916

2D Materials

PAPER

Electrical tuning of moiré excitons in $MoSe_2$ bilayers

Joakim Hagel[1,*], **Samuel Brem**[2] **and Ermin Malic**[1,2]

[1] Department of Physics, Chalmers University of Technology, 412 96 Gothenburg, Sweden
[2] Department of Physics, Philipps University of Marburg, 35037 Marburg, Germany
[*] Author to whom any correspondence should be addressed.

E-mail: joakim.hagel@chalmers.se

Keywords: moiré physics, excitons, TMD, optics, electric field

Supplementary material for this article is available online

OPEN ACCESS

RECEIVED
6 October 2022

REVISED
25 November 2022

ACCEPTED FOR PUBLICATION
5 December 2022

PUBLISHED
23 December 2022

Abstract

Recent advances in the field of vertically stacked 2D materials have revealed a rich exciton landscape. In particular, it has been demonstrated that out-of-plane electrical fields can be used to tune the spectral position of spatially separated interlayer excitons. Other studies have shown that there is a strong hybridization of exciton states, resulting from the mixing of electronic states in both layers. However, the connection between the twist-angle dependent hybridization and field-induced energy shifts has remained in the dark. Here, we investigate on a microscopic footing the interplay of electrical and twist-angle tuning of moiré excitons in $MoSe_2$ homobilayers. We reveal distinct energy regions in PL spectra that are clearly dominated by either intralayer or interlayer excitons, or even dark excitons. Consequently, we predict twist-angle-dependent critical electrical fields at which the material is being transformed from a direct into an indirect semiconductor. Our work provides new microscopic insights into experimentally accessible knobs to significantly tune the moiré exciton physics in atomically thin nanomaterials.

The realization of atomically thin nanomaterials, such as graphene and monolayers of transition metal dichalcogenides (TMDs), has opened up a new platform to study many-particle quantum phenomena [1–4]. Optical properties are of particular interest for TMDs, where strongly bound electron–hole pairs can form. They give rise to exciton features, which fundamentally change the optical response of the material [5–10]. By vertically stacking two TMD monolayers, long-lived interlayer excitons become possible, thus allowing for both the intralayer A exciton resonance (X_A) and the spatially separated interlayer exciton resonance (IX) in optical spectra [11–19], cf figure 1(a). Furthermore, the exciton can become strongly hybridized (hX in figure 1(a)) via interlayer carrier tunneling, and thus carry both an inter- and an intralayer component [20–23]. One example of strongly hybridized states are momentum-dark KΛ excitons, where the hole is located at the K valley and the electron resides in the Λ valley in the Brillouine zone. Due to the strong wavefunction overlap at the Λ valley, the electron is delocalized over both layers [22, 23].

Due to the charge separation of the interlayer exciton, it exhibits an out-of-plane dipole moment, allowing for external tuning via an electrical field for both the pure interlayer exciton as well as the hybrid exciton [24, 25]. Additionally, one can twist the TMD monolayers with respect to each other, which introduces a spatially periodic potential. At small twist angles, this moiré potential was shown to give rise to a flat band structure that traps excitons in real space [22, 26–33]. While experimental studies have shown that one can efficiently tune the optical properties of TMDs by applying an external out-of-plane electrical field [34–41], the interplay with the twist-angle-dependent tuning of exciton hybridization has not been explored microscopically. In this work, we investigate this interplay with a fully microscopic and material-specific theory based on the density-matrix formalism combined with first-principle calculations [22, 23, 33]. We predict twist-angle dependent critical electrical fields at which the $MoSe_2$ bilayer becomes an indirect semiconductor, where the dark KΛ exciton is clearly the energetically lowest state. The low-temperature PL spectrum

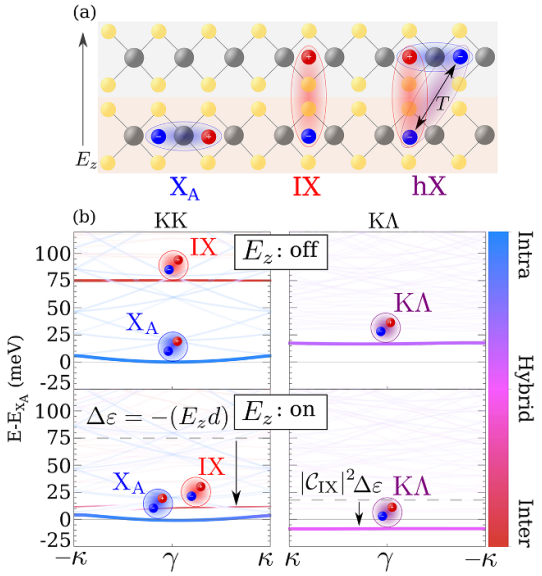

Figure 1. (a) Real space schematic for different exciton species in TMD bilayers including the intralayer exciton X_A, the interlayer exciton IX, and the hybrid exciton hX stemming from interlayer tunneling T. (b) Exciton band structure for R-type stacked $MoSe_2$ homobilyer for the bright KK (left) and dark KΛ excitons (right). Multiple moiré subbands are shown in faded colors. Only the interlayer and the hybrid exciton exhibiting a dipole moment become red-shifted in presence of an electrical field (lower panel). Dashed lines indicate the original position of the corresponding excitons without an electrical field. The calculation is performed for a twist angle of $\theta = 2°$ and an electrical field of $E_z = 0.1\ \mathrm{V\,nm^{-1}}$.

is then dominated by the phonon sidebands of this dark state. Depending on the electrical field and the twist-angle we find spectral regions, where either the intralayer X_A, the dark KΛ or the interlayer exciton IX are clearly dominating the PL spectrum.

1. Theoretical approach

To obtain a microscopic access to the optical response of moiré excitons, we first set up an excitonic Hamilton operator [22, 33, 42], using monolayer eigenstates as basis,

$$H_0 = \sum_{LQ\xi} E^{\xi}_{LQ}\, X^{\xi\dagger}_{L,Q}\, X^{\xi}_{L,Q} + \sum_{LQ\xi g} V^{\xi}_{Lg}\, X^{\xi\dagger}_{L,Q+g}\, X^{\xi}_{L,Q} + \sum_{LL'Q\xi g} T^{\xi}_{LL'g}\, X^{\xi\dagger}_{L,Q+g}\, X^{\xi}_{L',Q} + h.c, \quad (1)$$

where $L = (l_e, l_h)$ is the compound index for electron/hole layer $l_{e(h)}$, $\boldsymbol{Q}$ the center-of-mass momentum, and $\boldsymbol{\xi} = (\xi_e, \xi_h)$ the compound valley index allowing for both bright and momentum-dark excitons [43, 44]. Furthermore, $\boldsymbol{g}$ is the moiré lattice vector of the mini-Brillion zone (mBZ) [22, 33], while $X^{(\dagger)}$ are annihilation (creation) operators for layer localized excitons. The first term in equation (1) is the kinetic energy of excitons and includes their center-of-mass exciton dispersion as obtained by solving the bilayer Wannier equation [45]. The following two terms are twist-angle dependent, where V^{ξ}_{Lg} is the periodic polarization-induced interlayer alignment shift (here referred to as moiré-induced shift) taking into account the periodic modulation of interlayer excitons [33, 46]. Furthermore, $T^{\xi}_{LL'g}$ is the interlayer tunneling, taking into account the hybridization of electronic states in both layers [22, 23]. The moiré-induced shift and the hybridization both give rise to a periodic moiré potential that is present in TMD bilayers [47]. A complete derivation of the Hamiltonian and the appearing matrix elements is provided in the supplementary material.

To take into account the periodicity of the moiré superlattice, we apply a zonefolding approach and consequently restrict the summation over $\boldsymbol{Q}$ to the first mBZ [22, 33]. The moiré exciton band structure can be calculated by transforming the zone-folded Hamiltonian into a moiré exciton basis with the new exciton creation operators $Y^{\dagger}_{\xi\eta Q} = \sum_{gL} \mathcal{C}^{\xi\eta *}_{Lg}(\boldsymbol{Q}) X^{\xi\dagger}_{L,Q+g}$. The mixing coefficients $\mathcal{C}^{\xi\eta}_{Lg}(\boldsymbol{Q})$ contain the relative contribution of intra- and interlayer excitons as well the the contribution of each subband that emerges from twisting the structure. Here, η is the new moiré exciton band index. This transformation leads to the moiré exciton eigenvalue equation

$$E^{\xi}_{LQ+g}\mathcal{C}^{\xi\eta}_{Lg}(\boldsymbol{Q}) + \sum_{g'} V^{\xi}_{L}(\boldsymbol{g},\boldsymbol{g}')\mathcal{C}^{\xi\eta}_{Lg'}(\boldsymbol{Q}) + \sum_{L'g'} T^{\xi}_{LL'}(\boldsymbol{g},\boldsymbol{g}')\mathcal{C}^{\xi\eta}_{L'g'}(\boldsymbol{Q}) = \mathcal{E}^{\xi}_{\eta Q}\mathcal{C}^{\xi\eta}_{Lg}(\boldsymbol{Q}). \quad (2)$$

Solving this eigenvalue problem numerically gives a microscopic access to the hybrid moiré exciton energies $\mathcal{E}^{\xi}_{\eta Q}$ and the corresponding wave functions. This method is principally applicable to all TMD bilayers, but in this work, we focus on the exemplary case of $MoSe_2$ homobilayers that will turn out to be highly interesting.

Figure 1(b) shows the corresponding exciton band structure for the R-type stacked hBN-encapsulated $MoSe_2$ bilayer for a twist angle of $\theta = 2°$. The top panel shows the case without an electrical field and illustrates the bright KK excitons on the left and the dark KΛ excitons on the right. We find that at $\theta = 2°$, the A exciton is the energetically lowest lying state directly followed by the strongly hybridized dark KΛ exciton. Further up in the band structure, the interlayer IX exciton can be found. We predict that both the IX and the KΛ exciton exhibit very flat bands. This can be ascribed to the moiré-induced shift $V^{\xi}_{L}(\boldsymbol{g})$ that traps interlayer excitons in real space [33]. The same holds for KΛ excitons on top of a strong carrier tunneling, which is also periodic over the superlattice and contributes to the flatness of the band [22, 23]. The efficient tunneling of electrons at the Λ valley ($t_c^{\max} = 195$ meV [23]) is responsible for the pronounced hybrid nature of this exciton,

which exhibits nearly a 50/50 contribution from both its intra- and interlayer exciton components (cf the color gradient in figure 1(b). Furthermore, the solution of the moiré eigenvalue equation (2) also reveals the formation of multiple subbands emerging from the introduction of the twist angle and the resulting superlattice. The subbands stemming from the intralayer exciton (X_A) can then hybridize with the energetically higher interlayer IX exciton, cf the avoided crossings in the interlayer exciton in figure 1(b).

2. Moiré excitons in electrical fields

In presence of an out-of-plane electrical field, excitons become shifted in energy proportional to their dipole moment. The exciton-field interaction Hamiltonian reads

$$H_{X-l} = -\sum_{\boldsymbol{\xi} \mathbf{Q} L} d_L E_z X^{\boldsymbol{\xi}\dagger}_{\mathbf{Q},L} X^{\boldsymbol{\xi}}_{\mathbf{Q},L} \qquad (3)$$

with d_L as the dipole moment and E_z as the out-of-plane electrical field. Since this Hamiltonian is simply a renormalization of the potential energy of excitons, it can easily be incorporated into the first term of equation (1). Solving again the eigenvalue equation (equation (2)), we can now calculate the moiré exciton band structure in presence of an electrical field, cf the lower panel in figure 1(b) for the $MoSe_2$ bilayer at $\theta = 2°$ and $E_z = 0.1\ \mathrm{V\,nm^{-1}}$.

We predict that the interlayer exciton IX red-shifts in energy by $\Delta\varepsilon = -(E_z d)$ and becomes very close to the intralayer exciton X_A. Interestingly, we show clear avoided crossings with the higher-lying moiré subbands of X_A. As the states are nearly degenerate even the weak tunneling of carriers at the K point has a significant effect on the exciton band structure. There is also a field-induced red-shift of the dark KΛ exciton as it has an interlayer component (given by $|\mathcal{C}_{IX}|^2\Delta\varepsilon$) due to the strong hybridization. As a consequence, the KΛ exciton becomes the energetically lowest state at the considered twist angle of $\theta = 2°$, cf the lower panel of figure 1(b).

Now, we investigate how the exciton bands can be tuned with the electrical field in the untwisted R^M_h-stacked $MoSe_2$ bilayer, cf figure 2(a). At very low electrical fields, the dark KΛ exciton is found to be the lowest state, i.e. the untwisted $MoSe_2$ bilayer is an indirect semiconductor, however note that the bright X_A exciton is very close in energy. By introducing a twist angle (as in figure 1), the KΛ exciton lies above the bright exciton due to the reduced hybridization with the twist angle (caused by the momentum mismatch in the rotated Brilloine zones) [22, 31]. When increasing the electrical field, we observe a critical value of $E_z \approx 0.14\ \mathrm{V\,nm^{-1}}$ at which the interlayer exciton IX becomes the lowest lying state, cf figure 2(a). This is due to its larger effective dipole moment compared to the KΛ exciton (that is only partially interlayer-like) resulting in a steeper field-induced red-shift of the IX exciton. As the intralayer exciton X_A does not have a dipole moment and the hybridization is very weak at the K point, it remains unchanged in presence of an electrical field.

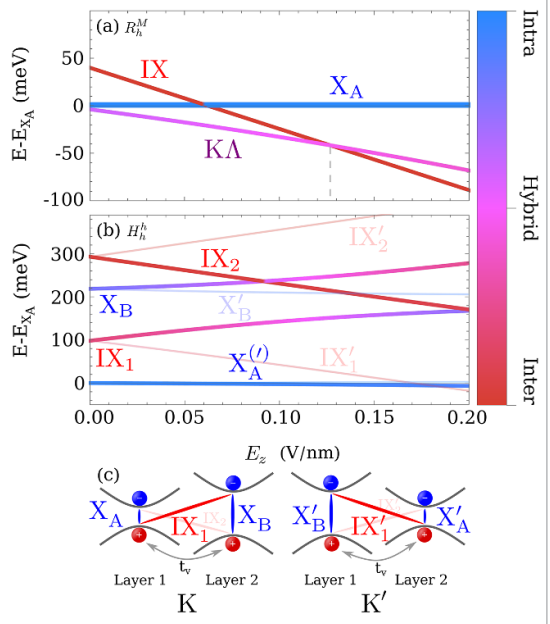

Figure 2. (a) Electrical field-induced tuning of exciton energy for the untwisted R^M_h-stacked $MoSe_2$ bilayer. The color gradient denotes the degree of hybridization between the intra- and interlayer excitons. The strongly hybridized KΛ exciton is the energetically lowest state in a certain E_z-range, while at even stronger fields the interlayer IX exciton becomes the lowest state. (b) Exciton band structure for H^h_h-stacked $MoSe_2$ bilayer. There is a strong hybridization between the field-shifted interlayer exciton IX_1 and the B exciton X_B (change of color at the avoided crossing). Shaded lines indicate the degenerate exciton species X′ that have the reversed dipole moment. (c) Schematic for the tunneling processes that couple different excitons in (b). $IX^{(\prime)}_1$ and $X^{(\prime)}_B$ couple with a strong hole tunneling t_v, while the hybridization is zero between $IX^{(\prime)}_2$ (shaded) and $X^{(\prime)}_B$ due to symmetry constraints. Note that IX_1 and IX'_1 have opposite dipole moments due to the reversed layer configuration of electrons and holes.

We have performed the same calculation for untwisted H^h_h-stacked $MoSe_2$ bilayers, cf figure 2(b). Due to the 180°-rotation of one of the layers in this stacking, the spin–orbit coupling in one of the layers is inverted [23]. This fundamentally changes the tunneling channels in comparison to R-type stacking. Here, we have the A exciton X_A in one layer coupling to the B exciton X_B in the other layer via the two interlayer states IX_1 and IX_2. There is also a degenerate exciton species X'_A (X'_b) with the reversed layer configuration that couple via their respective interlayer excitons IX'_1 (IX'_2). These interlayer excitons have the reversed dipole moment in comparison to IX_1 (IX_2), cf figure 2(c). Note that X and X′ states do not couple to each other via interlayer tunneling as these excitons are separated by large momentum in the Brillouin zone. These considerations plus the slight reduction of the interlayer distance for H^h_h stacking

(which increases the strength of the hole tunneling [23]) results in a significant hybridization between the energetically lowest interlayer exciton IX_1 and the B exciton X_B. The higher interlayer exciton IX_2 instead couples to the B exciton via electron tunneling (cf figure 2(c)), which is zero at this stacking due to the C3-symmetry at the K point (note that this symmetry only holds at $\theta = 0°$) [23]. By increasing the electrical field we find a slightly non-linear increase of X_B and IX_1 excitons. This can be ascribed to the fact that the tunneling strength between these excitons is in the same range as the shift induced by the electrical field. This allows for strong tuning of the mixing coefficients $C_{Lg}^{\xi\eta}(\boldsymbol{Q})$. The color gradient encodes the degree of hybridization and shows nicely the strong hybridization between X_B and IX_1 in the range around $E_z \approx 0.1\ \mathrm{V\,nm^{-1}}$ (pink color). Furthermore, due to the reversed dipole moment of the degenerate exciton species X', the interlayer excitons IX_1' (IX_2') are shifted in the opposite direction, as can be seen from the shaded lines in figure 2(b).

3. PL spectra of R-stacked $MoSe_2$ bilayers

Having obtained microscopic insights into the tunability of the exciton landscape with the electrical field in $MoSe_2$ bilayers, we now focus on the change of their optical response. We first calculate the PL spectrum of R-stacked bilayers and we explicitly consider also indirect phonon-driven exciton recombination processes [22, 48]. Here, momentum-dark states can become visible via scattering with a phonon to a virtual state within the light cone and resulting in the formation of phonon sidebands in PL spectra. These are expected to play an important role for R-stacked $MoSe_2$ bilayers, as here the momentum-dark KΛ excitons are the lowest states in a large range of electrical fields (cf figure 2(a)).

Figure 3 shows the PL spectrum for three different values of the electrical field E_z at $T = 4$ K. Without a field, the A exciton clearly dominates the PL. Even though the KΛ state is predicted to be slightly the lowest state, it is only so by a couple of meV (figure 2(a)). We do not observe here any phonon sidebands, as the phonon-assisted recombination is a higher-order process with a much smaller probability compared to the direct recombination. The predicted close proximity of the KΛ exciton to the bright A exciton according to the solution of the moiré eigenvalue equation agrees well with previous DFT studies [49] as well as with experimental data showing the dominance of the A exciton resonance [50].

By applying an electrical field we decrease the energy of the KΛ exciton pushing it far below the bright exciton. As a direct consequence, this dark state carries by far the largest occupation, which makes the phonon-assisted recombination dominate over the direct recombination process. At an electrical field of $E_z = 0.1\ \mathrm{V\,nm^{-1}}$, we find prominent phonon

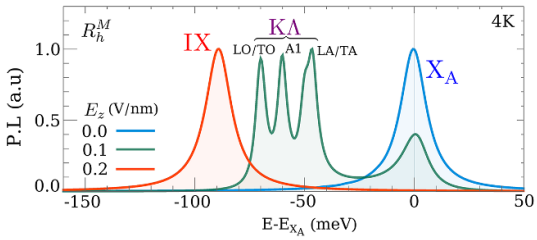

Figure 3. Photoluminescence spectrum for R_h^M-stacked $MoSe_2$ bilayers for three different electrical fields at 4 K. Without the field, the A exciton clearly dominates the PL and no other features are visible. When applying an out-of-plane electrical field ($E_z = 0.1\ (\mathrm{V\,nm^{-1}})$), the dark KΛ exciton is significantly red-shifted and its occupation becomes so large, that the phonon sidebands from this state dominate the PL. For even larger fields ($E_z = 0.2\ (\mathrm{V\,nm^{-1}})$), the strong red-shift of the interlayer exciton makes it to the lowest state and its emission dominates the PL.

sidebands from KΛ excitons, cf figure 3. The three distinct peaks stem from different phonon modes including the longitudinal/transverse optical modes (LO/TO), the A1 out-of-plane mode and the longitudinal/transverse acoustical modes (LA/TA). Since these are phonon-assisted processes, they are sensitive to temperature and they become less pronounced at higher temperatures. Increasing the electrical field further shifts the interlayer exciton IX (with the largest dipole moment and thus the steepest shift with the field) to the energetically lowest state (figure 2(a)). Consequently, the radiative recombination of the IX dominates the PL spectrum for large fields, cf figure 3.

In a similar fashion as in figure 2, we now investigate how the optical response of untwisted $MoSe_2$ bilayers evolves when continuously changing the electrical field, cf figure 4(a). At zero electrical field, the A exciton dominates the PL, however we observe a drastic change in the spectrum with just a slight increase of the field. Here, the KΛ exciton is sufficiently red-shifted to gain enough occupation to give rise to the clearly visible phonon sidebands. Due to the close proximity of the KΛ and the A exciton and the low temperature of $T = 4$ K, this change occurs rather abruptly. The phonon sidebands shift linearly with the electrical field due to the interlayer component of the strongly hybridized KΛ exciton. Around $E_z \approx 0.125\ \mathrm{V\,nm^{-1}}$, we predict another drastic change in the PL spectrum. Here, the interlayer exciton IX has become the energetically lowest state as it has a larger dipole moment than the KΛ exciton and thus exhibits a steeper shift with the electrical field (figure 2(a)). As the IX state is a bright exciton and recombines directly, we find again a single peak. It is blue-shifted with respect to the phonon sidebands of the KΛ exciton, since no phonon energy is involved in this recombination process.

Next we investigate how the field-induced tuning of the PL spectrum changes when introducing a

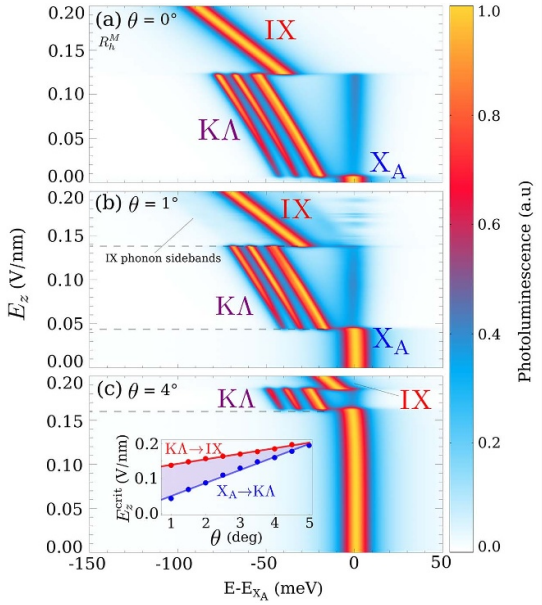

Figure 4. Photoluminescence spectra for R-type stacked $MoSe_2$ as a function of electrical field strength at the twist angles of (a) $\theta = 0°$, (b) $\theta = 1°$ and (c) $\theta = 4°$ at 4 K. We observe three distinct energy regions, which are dominated by the A exciton X_A, the phonon sidebands of the dark KΛ exciton and the interlayer exciton IX, respectively. The inset in (c) shows the critical electrical field strength E_z^{crit} as a function of the twist angle for the transition between different spectral regions (X_A to KΛ and X_A to IX-dominated region). The shaded area indicates the range, where the dark KΛ excitons dominate the PL.

finite twist angle and thus a moiré superlattice. We focus on twist angles of 1° or larger to avoid effects of atomic reconstruction [51]. For an angle of $\theta = 1.0°$, we find the qualitatively same drastic changes in the PL spectrum at specific critical field values, cf figure 4(b). Compared to the untwisted bilayer, there is an increased field range at which the A exciton dominates. The reason for this is an increased KΛ exciton energy in a twisted structure without electrical field. As result of the twist angle, the two monolayer band structures are rotated with respect to each other leading to an energetic detuning of hybridizing states. Moreover, the spatially varying stacking sequences result in variations of the interlayer distance, leading to a weaker tunneling than in the optimal R_h^M stacking discussed in figure 4(b). Further side effects leading to weaker hybridization with increasing twist angle have been discussed and experimentally observed in [31].

As a result of the above, it requires a larger electrical field to make this state energetically lowest and dominate the PL spectrum via its phonon sidebands. Furthermore, the rotation of the BZs leads to a energetic minimum of the interlayer exciton IX outside the light cone due to the momentum mismatch between the K points in the different layers. Consequently, there is a higher occupation in the finite-momentum regions of the interlayer exciton valley. This gives rise to some very weak phonon side bands of the IX exciton. The oscillations appearing at the energy of the X_Λ exciton stem from the hybridization of multiple IX subbands with the A exciton, cf also the avoided crossings in figure 1(b).

Further increasing the twist angle up to $\theta = 4°$, the field region with the dominant KΛ phonon sidebands has become very small, cf figure 4(c). Instead, the A exciton nearly dominates the entire energy range. KΛ and IX excitons become important only at relatively large fields of $E_z > 0.16\ \text{V nm}^{-1}$. This can again be ascribed to the decrease in the hybridization of KΛ excitons and the increased momentum-indirect character of the IX [33, 52], as discussed above. The inset in figure 4(c) describes the twist-angle dependent critical electrical field necessary to give rise to the drastic changes in the PL spectrum from spectral regions with a dominant X_A to KΛ (blue) as well as from KΛ to IX (red). We find that this critical field changes approximately linearly with the twist angle and that the transition X_A to KΛ has a steeper slope. This can be explained by the blue-shift of both excitons when increasing the size of the mBZ. Moreover, the KΛ exciton has a smaller effective dipole moment, making its slope less steep compared to the IX exciton. As a result, the KΛ dominated electric field region shrinks with increasing twist angle, cf the color-shaded region in the inset.

4. Absorption spectra of H-stacked bilayers

Finally, we investigate the H-stacked $MoSe_2$ bilayer. As in the R-type stacking, we find similar transitions in the PL for H-type stacked TMD bilayer, however unique for the H-type stacking is the strong hybridization between bright excitons. For this purpose, we focus on the optically accessible A and B excitons. The corresponding exciton band structure has already been discussed in figure 2(b), where it has been shown that the B exciton X_B strongly hybridizes with the interlayer exciton IX_1. Since both of these excitons are bright, but not the energetically lowest states, their PL signal is very small. Therefore, we now investigate the field-dependent optical response by studying the optical absorption as illustrated in figure 5 for different twist angles. In the untwisted case (figure 5(a)), we observe a very large avoided crossing between IX_1 and X_B, i.e. both lines become strongly non-linear when they come close to each other. This is due to the large hole tunneling around the K point ($t_v =$ 56 meV [23]), cf figure 2(c). As a result, the interlayer exciton IX_1 will be strongly hybridized and thus gains a considerable oscillator strength. This explains that the otherwise invisible interlayer exciton can be clearly observed in the absorption spectrum—in good agreement with previous experimental studies [36–38] and also in accordance with a previous DFT work [53]. Note that the IX_1' exciton, i.e the degenerate counterpart of IX_1 with reversed dipole moment (cf figure 2(c)) is not visible as it decreases with the

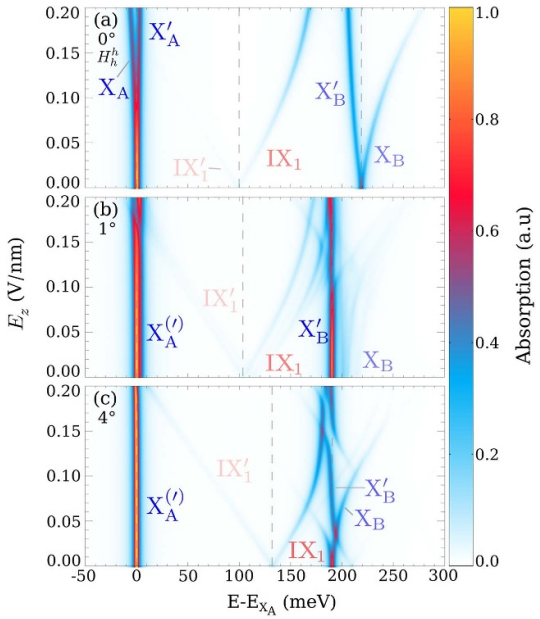

Figure 5. Absorption spectra for H-type stacked $MoSe_2$ as a function of electrical field E_z at the twist angles of (a) $\theta = 0°$, (b) $\theta = 1°$ and (c) $\theta = 4°$. We observe that the interlayer exciton IX_1 carries a considerable oscillator strength and has a pronounced avoided crossing with the B exciton. Dashed lines indicates the position of the peak without electrical field. Note that in contrast X_2 is not visible as here the hybridization with the X_B state is negligible, cf figure 2(b).

electrical field and is thus shifted away from its corresponding B exciton X'_B. Consequently, X'_B exciton remains almost unchanged under the electrical field. Furthermore, at very large electrical fields, we observe a small splitting of the two A excitons X_A and X'_A. This is as a consequence of its small interlayer component gained via hybridization with the interlayer exciton IX_2, which become closer with an increasing electrical field, cf figure 2(b).

Now, we go beyond previous studies and investigate how the optical response changes in H-stacked $MoSe_2$ bilayers, when a twist angle is introduced. We start with a small angle of $\theta = 1°$ (figure 5(b)). We find a qualitatively similar behavior as in the untwisted case, but with additional moiré subbands appearing in the spectrum. The higher subbands of the interlayer exciton are similarly affected by the electrical field and hybridize with the subbands of the B exciton X_B resulting in multiple avoided crossings. Moreover, also the intralayer B exciton is experiencing a superlattice potential resulting in a peak splitting due to the formation of moiré trapped states [33]. By further increasing the twist angle up to $\theta = 4°$ (figure 5(c)), most moiré subbands become dark due to a vanishing moiré induced mixing with lowest (bright) subband [33, 54]. Furthermore, we observe that the avoided crossing occurs at smaller values of the electrical field compared to the case of $\theta = 1°$. This is due to the interlayer exciton IX_1 being much closer to the B exciton X_B at higher twist angles. The other interlayer exciton IX'_1 is now more pronounced as it is closer to the B exciton and thus exhibits a stronger mixing/larger oscillator strength. Overall, the efficient hole tunneling between the interlayer exciton and the B exciton leads to a significant hybridization in H-stacked $MoSe_2$ bilayers, brightening up the otherwise invisible interlayer exciton. A twist angle introduces additional avoided crossings due to the hybridization with the appearing moiré subbands.

In conclusion, our work provides microscopic insights into the tunablity of moiré excitons with the electrical field and the twist angle in atomically thin semiconductors. In particular, we demonstrate the significant impact of the interlayer hybridization when applying an out-of-plane electrical field, predicting distinct spectral regions in PL spectra of R-stacked $MoSe_2$ bilayers, where the intralayer or the interlayer exciton or even the momentum dark KΛ exciton are clearly dominant. Consequently, we predict twist-angle-dependent critical electrical fields for the transition of the material from a direct into an indirect semiconductor. Overall, we shed light on microscopic many-particle processes behind the electrical tunability of moiré excitons in TMD bilayers, which can guide and trigger future experimental studies.

Data availability statement

All data that support the findings of this study are included within the article (and any supplementary files).

Acknowledgments

This project has received funding from Deutsche Forschungsgemeinschaft via CRC 1083 (Project B09) and the European Unions Horizon 2020 research and innovation programme under Grant Agreement No. 881603 (Graphene Flagship).

ORCID iD

Joakim Hagel https://orcid.org/0000-0002-3858-4174

References

[1] Ares P and Novoselov K S 2021 Recent advances in graphene and other 2D materials *Nano Mater. Sci.* **4** 3–9
[2] Tong Q, Yu H, Zhu Q, Wang Y, Xu X and Yao W 2017 Topological mosaics in moiré superlattices of van der Waals heterobilayers *Nat. Phys.* **13** 356
[3] Cao Y, Fatemi V, Fang S, Watanabe K, Taniguchi T, Kaxiras E and Jarillo-Herrero P 2018 Unconventional superconductivity in magic-angle graphene superlattices *Nature* **556** 43
[4] Sung J *et al* 2020 Broken mirror symmetry in excitonic response of reconstructed domains in twisted MoS_2/MoS_2 bilayers *Nat. Nanotechnol.* **15** 750

[5] Mueller T and Malic E 2018 Exciton physics and device application of two-dimensional transition metal dichalcogenide semiconductors *npj 2D Mater. Appl.* **2** 1

[6] Perea-Causin R, Erkensten D, Fitzgerald J M, Thompson J J, Rosati R, Brem S and Malic E 2022 Exciton optics, dynamics and transport in atomically thin semiconductors *APL Mater.* **10** 100701

[7] Splendiani A, Sun L, Zhang Y, Li T, Kim J, Chim C-Y, Galli G and Wang F 2010 Emerging photoluminescence in monolayer MoS_2 *Nano Lett.* **10** 1271

[8] He K, Kumar N, Zhao L, Wang Z, Mak K F, Zhao H and Shan J 2014 Tightly bound excitons in monolayer WSe_2 *Phys. Rev. Lett.* **113** 026803

[9] Chernikov A, Berkelbach T C, Hill H M, Rigosi A, Li Y, Aslan O B, Reichman D R, Hybertsen M S and Heinz T F 2014 Exciton binding energy and nonhydrogenic Rydberg series in monolayer WS_2 *Phys. Rev. Lett.* **113** 076802

[10] Wang G, Chernikov A, Glazov M M, Heinz T F, Marie X, Amand T and Urbaszek B 2018 Colloquium: excitons in atomically thin transition metal dichalcogenides *Rev. Mod. Phys.* **90** 021001

[11] Rivera P *et al* 2015 Observation of long-lived interlayer excitons in monolayer $MoSe_2$–WSe_2 heterostructures *Nat. Commun.* **6** 1

[12] Geim A K and Grigorieva I V 2013 Van der Waals heterostructures *Nature* **499** 419

[13] Liao W, Huang Y, Wang H and Zhang H 2019 Van der Waals heterostructures for optoelectronics: progress and prospects *Appl. Mater. Today* **16** 435

[14] Kunstmann J *et al* 2018 Momentum-space indirect interlayer excitons in transition-metal dichalcogenide van der Waals heterostructures *Nat. Phys.* **14** 801

[15] Miller B, Steinhoff A, Pano B, Klein J, Jahnke F, Holleitner A and Wurstbauer U 2017 Long-lived direct and indirect interlayer excitons in van der Waals heterostructures *Nano Lett.* **17** 5229

[16] Jin C, Ma E Y, Karni O, Regan E C, Wang F and Heinz T F 2018 Ultrafast dynamics in van der Waals heterostructures *Nat. Nanotechnol.* **13** 994

[17] Gillen R and Maultzsch J 2018 Interlayer excitons in mose 2/WSe_2 heterostructures from first principles *Phys. Rev.* B **97** 165306

[18] Merkl P *et al* 2019 Ultrafast transition between exciton phases in van der Waals heterostructures *Nat. Mater.* **18** 691

[19] Rivera P, Yu H, Seyler K L, Wilson N P, Yao W and Xu X 2018 Interlayer valley excitons in heterobilayers of transition metal dichalcogenides *Nat. Nanotechnol.* **13** 1004

[20] Alexeev E M *et al* 2019 Resonantly hybridized excitons in moiré superlattices in van der waals heterostructures *Nature* **567** 81

[21] Gerber I C *et al* 2019 Interlayer excitons in bilayer MoS_2 with strong oscillator strength up to room temperature *Phys. Rev.* B **99** 035443

[22] Brem S, Lin K-Q, Gillen R, Bauer J M, Maultzsch J, Lupton J M and Malic E 2020 Hybridized intervalley moiré excitons and flat bands in twisted WSe_2 bilayers *Nanoscale* **12** 11088

[23] Hagel J, Brem S, Linderälv C, Erhart P and Malic E 2021 Exciton landscape in van der Waals heterostructures *Phys. Rev. Res.* **3** 043217

[24] Jiang Y, Chen S, Zheng W, Zheng B and Pan A 2021 Interlayer exciton formation, relaxation and transport in TMD van der Waals heterostructures *Light Sci. Appl.* **10** 1

[25] Liu Y, Dini K, Tan Q, Liew T, Novoselov K S and Gao W 2020 Electrically controllable router of interlayer excitons *Sci. Adv.* **6** eaba1830

[26] Seyler K L, Rivera P, Yu H, Wilson N P, Ray E L, Mandrus D G, Yan J, Yao W and Xu X 2019 Signatures of moiré-trapped valley excitons in $MoSe_2$/WSe_2 heterobilayers *Nature* **567** 66

[27] Tran K *et al* 2019 Evidence for moiré excitons in van der Waals heterostructures *Nature* **567** 71

[28] Tong Q, Chen M, Xiao F, Yu H and Yao W 2020a Interferences of electrostatic moiré potentials and bichromatic superlattices of electrons and excitons in transition metal dichalcogenides *2D Mater.* **8** 025007

[29] Yu H, Liu G-B, Tang J, Xu X and Yao W 2017 Moiré excitons: from programmable quantum emitter arrays to spin–orbit-coupled artificial lattices *Sci. Adv.* **3** e1701696

[30] Zhang N, Surrente A, Baranowski M, Maude D K, Gant P, Castellanos-Gomez A and Plochocka P 2018 Moiré intralayer excitons in a $MoSe_2$/MoS_2 heterostructure *Nano Lett.* **18** 7651

[31] Merkl P *et al* 2020 Twist-tailoring coulomb correlations in van der Waals homobilayers *Nat. Commun.* **11** 1

[32] Kiemle J, Sigger F, Lorke M, Miller B, Watanabe K, Taniguchi T, Holleitner A and Wurstbauer U 2020 Control of the orbital character of indirect excitons in MoS_2/WS_2 heterobilayers *Phys. Rev.* B **101** 121404

[33] Brem S, Linderälv C, Erhart P and Malic E 2020b Tunable phases of moiré excitons in van der Waals heterostructures *Nano Lett.* **20** 8534

[34] Huang Z *et al* 2022 Spatially indirect intervalley excitons in bilayer WSe_2 *Phys. Rev.* B **105** L041409

[35] Altaiary M M, Liu E, Liang C-T, Hsiao F-C, van Baren J, Taniguchi T, Watanabe K, Gabor N M, Chang Y-C and Lui C H 1829 Electrically switchable intervalley excitons with strong two-phonon scattering in bilayer WSe_2 *Nano Lett.* **22** 2022

[36] Leisgang N *et al* 2020 Giant stark splitting of an exciton in bilayer MoS_2 *Nat. Nanotechnol.* **15** 901

[37] Peimyoo N *et al* 2021 Electrical tuning of optically active interlayer excitons in bilayer MoS_2 *Nat. Nanotechnol.* **16** 888

[38] Sponfeldner L, Leisgang N, Shree S, Paradisanos I, Watanabe K, Taniguchi T, Robert C, Lagarde D, Balocch A, Marie X, Gerber I C, Urbaszek B and Warburton R J 2021 Capacitively-coupled and inductively-coupled excitons in bilayer MoS_2 (arXiv:2108.04248)

[39] Wang Z, Chiu Y-H, Honz K, Mak K F and Shan J 2018 Electrical tuning of interlayer exciton gases in WSe_2 bilayers *Nano Lett.* **18** 137

[40] Ramasubramaniam A, Naveh D and Towe E 2011 Tunable band gaps in bilayer transition-metal dichalcogenides *Phys. Rev.* B **84** 205325

[41] Wu S *et al* 2013 Electrical tuning of valley magnetic moment through symmetry control in bilayer MoS_2 *Nat. Phys.* **9** 149

[42] Katsch F, Selig M, Carmele A and Knorr A 2018 Theory of exciton–exciton interactions in monolayer transition metal dichalcogenides *Phys. Status Solidi* b **255** 1800185

[43] Malic E, Selig M, Feierabend M, Brem S, Christiansen D, Wendler F, Knorr A and Berghäuser G 2018 Dark excitons in transition metal dichalcogenides *Phys. Rev. Mater.* **2** 014002

[44] Berghäuser G, Steinleitner P, Merkl P, Huber R, Knorr A and Malic E 2018 Mapping of the dark exciton landscape in transition metal dichalcogenides *Phys. Rev.* B **98** 020301

[45] Ovesen S, Brem S, Linderälv C, Kuisma M, Korn T, Erhart P, Selig M and Malic E 2019 Interlayer exciton dynamics in van der Waals heterostructures *Commun. Phys.* **2** 1

[46] Tong Q, Chen M, Xiao F, Yu H and Yao W 2020 Interferences of electrostatic moiré potentials and bichromatic superlattices of electrons and excitons in transition metal dichalcogenides *2D Mater.* **8** 025007

[47] Linderälv C, Hagel J, Brem S, Malic E and Erhart P 2022 The moiré potential in twisted transition metal dichalcogenide bilayers (arXiv:2205.15616)

[48] Brem S, Ekman A, Christiansen D, Katsch F, Selig M, Robert C, Marie X, Urbaszek B, Knorr A and Malic E 2020 Phonon-assisted photoluminescence from indirect excitons in monolayers of transition-metal dichalcogenides *Nano Lett.* **20** 2849

[49] Deilmann T and Thygesen K S 2019 Finite-momentum exciton landscape in mono-and bilayer transition metal dichalcogenides *2D Mater.* **6** 035003

[50] Liu H J, Jiao L, Xie L, Yang F, Chen J L, Ho W K, Gao C L, Jia J F, Cui X D and Xie M H 2015 Molecular-beam epitaxy of monolayer and bilayer WSe_2: a scanning tunneling microscopy/spectroscopy and deduction of exciton binding energy *2D Mater.* **2** 034004
[51] Enaldiev V, Zólyomi V, Yelgel C, Magorrian S and Fal'ko V 2020 Stacking domains and dislocation networks in marginally twisted bilayers of transition metal dichalcogenides *Phys. Rev. Lett.* **124** 206101
[52] Choi J *et al* 2021 Twist angle-dependent interlayer exciton lifetimes in van der Waals heterostructures *Phys. Rev. Lett.* **126** 047401
[53] Deilmann T and Thygesen K S 2018 Interlayer excitons with large optical amplitudes in layered van der Waals materials *Nano Lett.* **18** 2984
[54] Fitzgerald J M, Thompson J J and Malic E 2022 Twist angle tuning of moiré exciton polaritons in van der Waals heterostructures *Nano Lett.* **22** 4468–74